

Controlling failure regimes in Brick-and-Mortar structures

Georgia Hunter¹, Lee Djumas¹, Laurence Brassart^{1,2}, Andrey Molotnikov^{1,3}

¹Department of Materials Science and Engineering, Monash University, Clayton, Australia

²Department of Engineering Science, University of Oxford, Oxford, UK

³RMIT Centre for Additive Manufacturing, School of Engineering, RMIT University, Melbourne, Australia
e: Georgia.Hunter@monash.edu

Abstract

Brick-and-Mortar structures have a highly tunable mechanical response, offering the possibility to achieve exceptional combinations of properties such as strength and toughness. These properties markedly depend on the failure mechanism. However, the effect of geometric and material parameters on failure is not fully understood. In this work we report the existence of a ‘two-peak’ and a ‘peak-plateau-peak’ failure regime, differing in the ability of the structure to distribute damage in the layers prior to failure. A transition from the ‘two-peak’ to ‘peak-plateau-peak’ regime is observed in 3D-printed Brick-and-Mortar structures by increasing the aspect ratio (brick width over height) in the lower “layer failure” aspect ratio range. Further control of the two regimes is investigated with the help of a semi-analytical model of finite-sized structures. Theoretical predictions suggest that the failure regime can be controlled by tuning the relative shear and normal layer materials. This is confirmed experimentally by testing Brick-and-Mortar structures made with different materials for the shear and normal layers. Our work demonstrates that the transition from the ‘two-peak’ to the ‘peak-plateau-peak’ failure regime significantly increases the toughness, without compromising strength or stiffness of the structure, highlighting the importance of controlling these regimes.

Keywords

Composites

Toughness

Nacre

Bioinspired

Micromechanical modelling

Architected materials

1. Introduction

Natural materials often exhibit exceptional combinations of properties that are commonly mutually exclusive in man-made structures [1, 2]. For example, nacre [3], conch shells [4], stomatopod dactyl club [5], bone [6], dentin [1] and wood [7] all display a remarkable combination of strength and toughness. The exceptional combinations of properties often arise from the arrangement of stiff and soft materials in a specific geometric design motif [8, 9]. One particular design motif of interest is the *Brick-and-Mortar* arrangement, which combines stiff discrete bricks in a periodically staggered arrangement joined together by thin layers of soft material [10].

Additive Manufacturing has been used extensively to investigate these structures [11-21] due to the high level of spatial control possible and ability to manufacture multi-material structures. One of the earliest replications of the Brick-and-Mortar structure via Additive Manufacturing confirmed that the exceptional combinations of properties in these structures arises from the geometric arrangement of the materials [12].

Further investigation into these structures has shown that they not only have exceptional combinations of strength and toughness, but that they also exhibit a highly tunable mechanical response. This is due to the large number of design parameters associated with the structure, including their geometric [11, 12, 15, 22-30] and material [18, 23, 28, 31] parameters, and the control of design over multiple length scales [11, 17, 20, 32]. Their tunable response extends the existing design parameter space, broadening the possible applications for this type of structure.

Understanding how design parameters affect the failure mechanism of Brick-and-Mortar structures is important for controlling and predicting their strength and toughness. Previous experimental and modelling efforts have revealed the existence of a distinctive transition in the failure regime from failure through the soft layers to failure through the stiff bricks, by either increasing the aspect ratio of the bricks [33], decreasing the volume fraction of the soft phase [33] or decreasing the stiffness contrast between the stiff and soft material [18],[31]. To better understand the full spectrum of possible failure regimes, Begley et al. [23] developed a 2D analytical model to generate a failure map spanning across a large range of parameters. In their model, the structure is modelled as a periodic unit cell consisting of two bricks, the layers perpendicular to the loading direction (normal layers) and the layers parallel to the loading direction (shear layers). The failure sequence under uniaxial loading is defined by yielding and

failure of each of the constituents. This modelling predicts a transition from layer failure to brick failure, and further that, within the layer failure regime, there are multiple failure regimes possible depending on the order of yielding and failure of the normal and shear layers. The model predicts that these different regimes are controlled by brick aspect ratio, the relative shear and normal strength of the material and the volume fraction. However, these regimes have not been explored and validated experimentally.

In this work we experimentally explore the parameter space of 3D-printed Brick-and-Mortar structures by tuning their aspect ratio in the “layer failure” range as previously identified by Begley et al [23]. Our work identified two regimes that have not been previously reported. The first failure regime, which we denote a ‘two-peak’ failure response, is characterised by failure first occurring through a pair of adjacent rows of normal layers, followed by failure of the shear layers that join the failed normal layers. The second failure regime, which we denote a ‘peak-plateau-peak’ failure response, involves the progressive failure of normal layers followed by the failure of the shear layers once all the normal layers have failed.

These two regimes cannot be predicted by an elementary periodic unit cell analytical model as used previously in the literature, since it assumes that all the normal layers fail simultaneously, and all the shear layers fail simultaneously. To overcome this shortcoming, we proposed and developed a new semi-analytical model, which considers the Brick-and-Mortar structure as a finite-size system. This model can predict the new failure regimes, and demonstrates that the regimes can be controlled by both the aspect ratio and the relative shear and normal layer parameters. This is confirmed with experiments where different materials are used for the shear and normal layers to control the interface strength ratio. To the best of our knowledge, structures with different shear and normal layers properties have not been investigated before. We show analytically, and verify experimentally, that the toughness of the structure significantly increases as we transition from a ‘two-peak’ failure response to a ‘peak-plateau-peak’ failure response, without compromising its strength and stiffness. These findings have important implications for the design of multi-material structures with tunable mechanical response.

2. Experiments

2.1 Design and Fabrication

Brick-and-Mortar structures with stiff rectangular bricks joined by a soft interfacial layer were designed and fabricated to be tested under uniaxial tension for determination of their mechanical response and failure sequence, see Figure 1a. The number of bricks in each direction was chosen based on previous studies of similar structures, fabricated with the same additive manufacturing technique and materials, and tested under similar loading conditions [13]. The selected geometry of a sample consists of five bricks in the loading direction, ten bricks in the perpendicular in-plane direction and a single brick in the out-of-plane direction.

Geometrically, the rectangular bricks are defined by their length (w) and height (h) and the normal and shear layers are described by their in-plane thickness (t), see Figure 1a. These parameters can be represented by two dimensionless parameters; Brick aspect ratio ($A_R = w/h$) and brick height to layer thickness ratio (h/t). A range of aspect ratios between 2 and 8.5 were considered in the experiments to capture the possible failure regimes. All other parameters were kept constant to ensure the effect of changing the aspect ratio was isolated; the normal and shear layer in-plane thickness was kept constant at 0.25mm, the brick height to layer thickness ratio was kept constant at 8.8 and the out-of-plane thickness of the structure was kept constant at 3.125mm. These values were chosen based on other studies of similarly manufactured and tested Brick-and-Mortar structures [11, 12, 18].

All structures were fabricated with the Objet Connex500 3D printer (Stratasys, Ltd.). This is a polymer jetting 3D printer that can create multi-material parts with chemically bonded, interfacial joins between the different materials. This type of printer has been used extensively to fabricate Brick-and-Mortar structures [11-21] due to the high spatial control and the strong interfacial bond between different materials. The materials printable with this printer include a stiff and rigid polymer, VeroWhitePlus (VW+), and a soft and rubbery polymer, TangoBlackPlus (TB+). The printer can also produce Digital Materials with a variety of shore properties by mixing distinctive resins such as VW+ and TB+. Some examples of predominantly TB+ Digital Materials are DM70 and DM85, listed with increasing proportion of VW+, and listed with increasing strength. Representative properties for TB+, DM70, DM85 and VW can be found in the Supplementary Information (SI 2). In this study, the Brick-and-Mortar structures were primarily fabricated with VW+ bricks, and TB+ layers, due to their

large contrast in properties. To demonstrate the identified failure regimes could be controlled by changing the respective shear and normal layer material, a Brick-and-Mortar structure was manufactured with TB+ in the normal layers and DM85 in the shear layers. Furthermore, a third structure with TB+ normal layers and DM70 shear layers was also experimentally tested, to validate the prediction of composite trends. DM70 and DM85 were chosen for these tests as they are still predominantly TB+ and therefore they still have a large enough contrast in properties with the VW+ bricks to ensure failure through the layers, but their mixing with a small amount of VW+ means that they are stronger than TB+, allowing us to observe the effect on the failure regime when the shear layer material is stronger than the normal layer material.

A summary of the structures fabricated for testing, and the respective aspect ratio and shear layer material for each, is listed in Table 1.

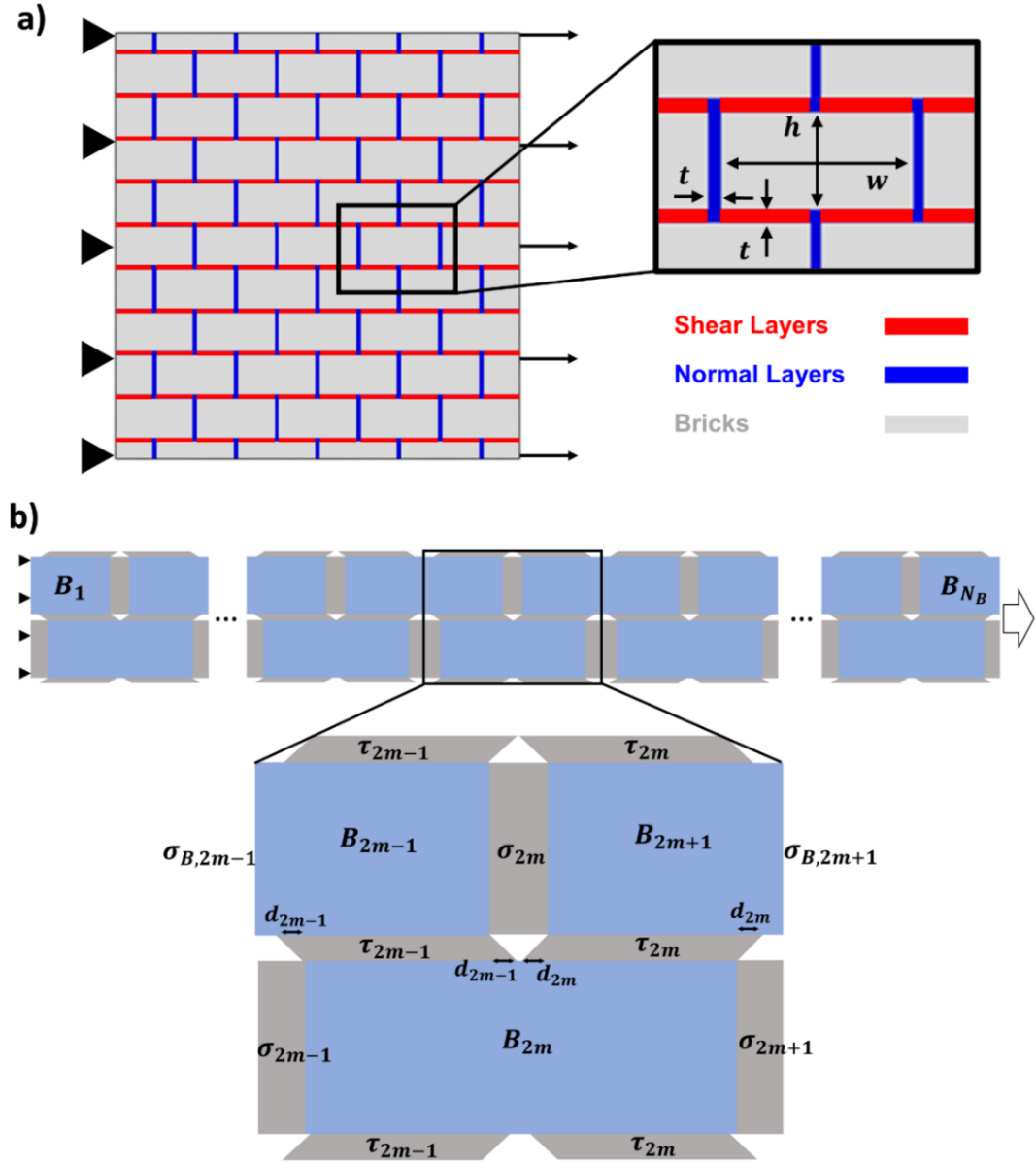


Figure 1: a) Schematic representation of a Brick-and-Mortar structure under uniaxial loading and the defining geometric parameters of the structure. b) A schematic of the finite-sized representative geometry of the Brick-and-Mortar structure with a finite number N_B of rigid bricks. The structure is assumed periodic in the vertical direction. The structure is shown in its deformed state to illustrate the deformed shape of the soft layers. A single unit cell (cell m in the structure) is highlighted to show the nomenclature used to define the brick number, the relative displacements between bricks and the normal and shear stresses in the soft layers.

Table 1: Parameters of Brick-and-Mortar structures experimentally tested.

Brick-and-Mortar Structure Name	Aspect Ratio ($A_R = \frac{w}{h}$)	Normal Layer Material	Shear Layer Material
AR2	2	TB+	TB+
AR2.5	2.5	TB+	TB+
AR4.5	4.5	TB+	TB+
AR6.1	6.1	TB+	TB+
AR8.5	8.5	TB+	TB+
DM85	2.5	TB+	DM85
DM70	2.5	TB+	DM70

2.2 Mechanical Testing

The Brick-and-Mortar structures were all tested under uniaxial tension using the Instron E3000 with a 3kN load cell. All samples were tested in a minimum of triplicate and tested within 24-36 hours of printing, to minimise the effect of ageing time reported in literature [34] allowing reliable comparison between samples. Due to the known rate-dependency of the materials printable on the Connex [16, 35], all structures were tested so that the layers, which are assumed to contribute to the majority of the strain, were under the same, low, strain rate for all samples. As there are the same number of layers in each structure, and they are all of the same thickness, this was achieved by keeping the displacement rate for the different structures the same: 0.4mm/min.

3. Semi-Analytical Modelling

We developed a semi-analytical model to gain insight into the failure mechanisms of the Brick-and-Mortar structures. In the presentation below, we first develop a simple model based on a single unit cell using a similar analysis to the work by Begley et al [23, 28]. The model is then extended to multiple unit cells, which allows us to capture the finite size effects and to introduce flaws to trigger localised damage. As shown below, accounting for distributed damage via a multi-cell representative element is essential to understand and capture the full range of failure regimes possible in the structure.

We first consider a single unit cell with three bricks, as highlighted in Figure 1b (ie. taking $N_B = 1$). The left-hand side of the cell is fixed, and the right-hand side of the cell is subjected to a prescribed horizontal displacement. The unit cell consists of three types of geometric entities: the rectangular bricks, the layers that are perpendicular to the loading direction and the layers that are parallel to the loading direction. Under an uniaxial displacement, the layers perpendicular to the loading direction are purely under normal stress and will thus be labelled ‘normal layers’ going forward, while the layers parallel to the loading direction are purely under shear stress and will thus be labelled ‘shear layers’ going forward. To simplify the analysis, bricks are assumed to be rigid, and the layer response is described by a Cohesive Zone Model (CZM) with bilinear traction-separation law, thus encompassing the deformation and damage response simultaneously.

The traction separation law of the normal layer is specified via the following parameters: an effective normal moduli (E_n), a normal strength (σ_{max}), and a normal fracture energy (G_{IC}). Likewise, the traction-separation law of a shear layer is specified via the effective shear moduli (E_s), shear strength (τ_{max}) and shear fracture energy (G_{IIC}). Traction separation laws relate the normal and shear stresses to the normal and shear opening displacement of the layers, respectively, and can be written in the following form:

$$\sigma = E_n^* \frac{\Delta d_n}{t} \quad (1)$$

$$\tau = E_s^* \frac{\Delta d_s}{t} \quad (2)$$

Where σ is the normal stress in the normal layer and Δd_n its opening displacement, and τ is the shear stress in the shear layer and Δd_s its opening displacement. E_n^* and E_s^* represent damaged normal and shear modulus, and are given by:

$$E_n^* = E_n(1 - D_n), \quad E_s^* = E_s(1 - D_s) \quad (3)$$

Where D_n and D_s are damage variables that evolve monotonically from 0 to 1 once the strength of the normal or shear layer, respectively, is reached. See SI for more details on the CZM (SI 1).

Consider the unit cell subjected to a prescribed total displacement d_T corresponding to a macroscopic, composite strain $\varepsilon_T = d_T/(w + t)$. Under the applied load, the Brick B_2 moves by a displacement d_1 relative to Brick B_1 , and Brick B_3 moves by a displacement d_2 relative to Brick B_2 . Since the bricks are rigid, we have the kinematic condition: $d_T = d_1 + d_2$. Identification of the two relative displacements is achieved from the consideration of force balance on Brick B_2 , giving the additional relation: $\sigma_1 h + \tau_1 w = \sigma_3 h + \tau_2 w$. Inserting the traction-separation relations (1,2), this gives the condition:

$$-d_1(2E_n^* h + E_s^* w) + d_2(2E_n^* h + E_s^* w) = 0 \quad (4)$$

Consideration of force balance on brick B_3 allows us to calculate the normal stress in the brick from the condition: $\sigma_{B,3} h = \sigma_2 h + \tau_2 w$. The macroscopic composite stress can then be calculated on the loading edge as:

$$\sigma_C = \frac{\sigma_{B,3} h + \sigma_3 h}{2h} = \frac{\sigma_2 h + \tau_2 w + \sigma_3 h}{2h} \quad (5)$$

According to the model, full failure (reached when the macroscopic stress drops to zero) occurs when there is an uninterrupted line of failed layers.

We now generalize the approach to a system of N_C juxtaposed unit cells, which interact via normal stress continuity across their cell boundary. To allow the introduction of a defect in the system, each layer is assigned its own set of CZM parameters which can be separately controlled, ie. the i th shear layer is assigned the parameters $E_{s,i}$, $\tau_{max,i}$, $G_{II,i}$ and the i th normal layer is assigned the parameters $E_{n,i}$, $\sigma_{max,i}$, $G_{I,i}$. The damage variable for each layer also evolves separately: $D_{n,i}$ for the i th normal layer and $D_{s,i}$ for the i th shear layer. Damaged moduli in the layers are defined as: $E_{n,i}^* = E_{n,i}(1 - D_{n,i})$ and $E_{s,i}^* = E_{s,i}(1 - D_{s,i})$. The traction-separation laws relating stresses in the i th normal (σ_i) and i th shear layer (τ_i) to the i th displacement can be written in the following form:

$$\sigma_i = \begin{cases} \frac{2E_{n,i}^* d_i}{t}, & i = 1 \\ \frac{E_{n,i}^* (d_{i-1} + d_i)}{t}, & i = 2, 3, \dots, 2N_C \\ \frac{2E_{n,i}^* d_{i-1}}{t}, & i = 2N_C + 1 \end{cases} \quad (6)$$

$$\tau_i = \frac{E_{s,i}^* d_i}{t}, \quad i = 1, 2, \dots, N_C \quad (7)$$

In the multi-cell construction, we now have $2N_C$ unknown relative displacements. Force balance on the middle bricks of each cell gives N_C relations: $\sigma_{2m-1}h + \tau_{2m-1}w = \sigma_{2m+1}h + \tau_{2m}w$, for $m = 1, 2, \dots, N_C$. Force balance on the bricks shared across cell boundaries gives another $N_C - 1$ relations: $\sigma_{2m}h + \tau_{2m}w = \sigma_{2m+2}h + \tau_{2m+1}w$, for $m = 1, 2, \dots, N_C - 1$. Inserting the traction-separation relations (6,7), this gives the following set of $2N_C - 1$ linear equations:

$$\begin{aligned} -(2E_{n,1}^* h + E_{s,1}^* w)d_1 + (E_{n,3}^* h + E_{s,2}^* w)d_2 + E_{n,3}^* h d_3 &= 0 \\ -E_{n,i}^* h d_{i-1} - (E_{n,i}^* h + E_{s,i}^* w)d_i + (E_{n,i+2}^* h + E_{s,i+1}^* w)d_{i+1} + E_{n,i+2}^* h d_{i+2} &= 0, \quad i = 2, 3, \dots, 2N_C - 2 \\ -E_{n,2N_C-1}^* h d_{2N_C-2} - (E_{n,2N_C-1}^* h + E_{s,2N_C-1}^* w)d_{2N_C-1} + (2E_{n,2N_C+1}^* h + E_{s,2N_C}^* w)d_{2N_C} &= 0 \end{aligned} \quad (8)$$

In addition, we have the kinematic relation: $d_T = \sum_{i=1}^{2N_C} d_i$. This gives a total of $2N_C$ linear algebraic relations which can be represented in matrix form to easily solve for $2N_C$ displacements for a known prescribed displacement d_T .

Consideration of force balance on brick B_{2N_C+1} ($= B_{N_B}$) allows us to calculate the normal stress in the brick from the condition: $\sigma_{B,2N_C+1}h = \sigma_{2N_C}h + \tau_{2N_C}w$. The macroscopic composite stress can then be calculated on the loading edge as:

$$\sigma_C = \frac{\sigma_{B,2N_C+1}h + \sigma_{2N_C+1}h}{2h} = \frac{\sigma_{2N_C}h + \tau_{2N_C}w + \sigma_{2N_C+1}h}{2h} \quad (9)$$

When all the normal and shear layer parameters take the same value across the structure, the response of the multi-cell structure is identical to the single-cell one, and therefore of no further interest. The benefit of the multi-cell structure is that it allows the simulation of progressive damage across the structure, triggered by localised damage. In practice, a small ‘defect’ was introduced in the model by reducing the strength of the middle layer (ie. σ_{max,N_C+1}) by 0.1% compared to the other normal layers in the structure. A defect size sensitivity analysis is provided in the Supplementary Information (SI 3).

It was found that the number of cells did not affect the predicted failure mechanism in the semi-analytical model, and therefore a finite number of 10 cells was chosen to show a representative behaviour (see SI 4 for more information on the size effect study).

To accurately model the experimental tests with the semi-analytical model, calibration of the normal and shear CZM parameters for the TB+, DM70 and DM85 materials was completed via uniaxial testing of a Layered Tensile Test (LTT) and a Single Lap Joint (SLJ) samples. The tested samples were specially designed to capture the true material response of the layers in the Brick-and-Mortar structure (see SI 2 for further details on the design of these tests). The calibrated parameters for TB+, DM70 and DM85 are shown in Table 2.

Table 2: Calibrated CZM Parameters for PolyJet materials TB+, DM70 and DM85

Material	E_n (MPa)	E_s (MPa)	σ_{max} (MPa)	τ_{max} (MPa)	G_{IC} (MPa.mm)	G_{IIC} (MPa.mm)
TB+	14	1.25	6.5	2.75	1	1
DM70	14	3	12.5	6.5	2	3
DM85	14	3.5	17	8	4.25	4.25

4. Results and Discussion

The stress-strain response for the two different aspect ratio Brick-and-Mortar structures, AR2.5 and AR6.1, is shown in Figure 2, along with snapshots taken at high deformation stages. The structure exhibits two distinct stress-strain responses, corresponding to distinct failure regimes. For both aspect ratios, the first peak in the stress-strain response (Point A on the figure) corresponds to the first damage in the normal layers. First damage, and subsequent failure, is observed to occur within only a couple of rows of the normal layers first, and not throughout the whole structure. Subsequent failure events then differ in the two structures:

- For the smaller aspect ratio (AR 2.5) the next failure event is shear layer failure between the already failed normal layers, which corresponds to the second peak in the stress-strain response (Point B). This results in an uninterrupted line of failure through the structure, thus leading to full failure of the structure (Point C). As there are only two failure events, correlating to two distinct peaks in the stress-strain response, we will denote this as a ‘two-peak’ failure response.
- For the larger aspect ratio (AR 6.1), after the first couple of rows of normal layers have failed, the next failure event is sequential failure of the normal layers, propagating out from the failure of the first couple of failed normal layers. This progressive failure of the rows of normal layers corresponds to the plateau in the stress-strain response. The second linear increase in the plot corresponds to the time between all the normal layers having failed and failure of the shear layers, as evidenced in snapshot B. The second peak then corresponds to the failure of the shear layers, resulting in failure of the structure (Point C). Due to the resulting shape of the stress-strain response, we will denote this failure regime a ‘peak-plateau-peak’ failure response.

The two failure regimes characterise the ability of the structure to distribute damage prior to failure. The ‘two-peak’ failure response is unable to distribute damage effectively while the ‘peak-plateau-peak’ failure response is. In literature to date, there have only been two distinct failure regimes identified experimentally for Brick-and-Mortar structures under this loading condition: failure through the layer or failure through the bricks [18, 31, 33]. Here we have shown that even within the failure regime of failure through the layers, there are additional distinguishing failure regimes possible for Brick-and-Mortar structures.

The semi-analytical model was interrogated to examine the prediction of the model with and without the introduction of flaws and the results are summarised in Figure 3a. It can be seen that the predicted stress-strain response drastically changes with the introduction of a flaw. Most significantly, the model with the flaw can predict the two new failure regimes that we identified experimentally. Allowing for different damage states in the layers in the semi-analytical model with the pre-existing flaw reveals a failure sequence for each aspect ratio which follows the experimentally observed trend. The AR 2.5 structure fails first in the normal layer with the defect and its directly adjacent normal layers, followed by failure of the shear layer that joins up the failed normal layers. While the AR 6.1 structure fails first in the normal layer with the defect and its directly adjacent normal layers, followed by progressive failure of the normal layers, and then failure of the shear layers once all the normal layers have failed. In contrast, the same model without pre-existing flaw fails to capture the experimental trends. These observations suggest that failure is related to the presence of flaws in the structure, and further highlights the need for models to account for the presence of flaws in order to accurately reproduce the response of Brick-and-Mortar structures.

The semi-analytical model also predicts a third possible failure regime where the shear layers fail first, thus resulting in instantaneous failure of the structure, which we label ‘shear-only’ failure. We do not observe this failure type experimentally due to the limited range of parameters for which this mechanism occurs. A fourth possible failure regime is linked to failure through the bricks and could be accounted for by introducing damage criterion for the stiff brick material into the model. However, this failure type is not further investigated since it has already been reported in previous studies.

Using the semi-analytical model, we derived analytical criteria to predict how the structure parameters affect the failure regimes (derivation shown in SI 5):

$$\text{'Shear-only' failure if: } \sigma_R < \frac{1}{2E_R} \quad (10)$$

$$\text{'Two-peak' failure if: } \frac{1}{2E_R} < \sigma_R < \frac{1}{2E_R} + \frac{1}{A_R} + \frac{1}{2(E_R + A_R)} \quad (11)$$

$$\text{'Peak-plateau-peak' failure if: } \sigma_R > \frac{1}{2E_R} + \frac{1}{A_R} + \frac{1}{2(E_R + A_R)} \quad (12)$$

$$\text{where } A_R = \frac{w}{h}, E_R = \frac{En}{E_s}, \sigma_R = \frac{\tau_{\max}}{\sigma_{\max}}.$$

Figure 3b shows a visual representation of the interplay between three identified parameters A_R , E_R and σ_R on the failure regime via two 2D variable maps of A_R vs E_R for σ_R values of 0.1 and 0.25. The boundary between failure regimes is captured with a solid, black line and colours are used to identify the failure regime for each region: brown for ‘shear-only’ failure, green for ‘two-peak’ failure and purple for ‘peak-plateau-peak’ failure.

From the analytical criteria, we note that the failure regime is not only controlled by changing the aspect ratio of the bricks, as already experimentally observed, but by also controlling the relative shear and normal layer material parameters. Specifically, we can transition from ‘two-peak’ failure to ‘peak-plateau-peak’ failure by increasing the strength of the shear layers relative to the strength of the normal layers. To test this hypothesis, we have fabricated and tested a Brick-and-Mortar structure with TB+ normal layers and DM85 shear layers, see Figure 4. The results of these experiments clearly show the structure with the stronger (DM85) shear layers exhibits ‘peak-plateau-peak’ failure, as evidenced by failure of all the normal layers prior to full failure of the structure, while the TB+-only structure exhibits ‘two-peak’ failure, as evidenced by the sudden full failure of the structure immediately after the first couple of normal layers have failed.

An important trend that is observed for the transition from ‘two-peak’ failure to ‘peak-plateau-peak’ failure is an increase in the area under the stress-strain curve (ie. defined here as toughness (T)) without compromising on the strength (σ_Y) or stiffness (E_{comp}) of the composite structure, which is a result of the ability of the structure to better distribute damage prior to failure. This trend is observed in the experiments for different aspect ratio, where we observe an 8-fold increase in toughness from the AR2.5 structure with a ‘two-peak’ failure response to the AR 6.1 structure with a ‘peak-plateau-peak’ failure response, see Figure 5. The trend is also observed in the experiments for different shear layer material, where we observe an 11-fold increase in toughness from the TB+ structure with a ‘two-peak’ failure response to the DM85 structure with a ‘peak-plateau-peak’ failure response, see Figure 5. In both of these cases the yield stress and moduli increase, demonstrating that the increase in toughness does not compromise the composite strength or stiffness. We validated that this trend holds for all parameters by developing analytical relations for the composite parameters and composite properties. Refer to the Supplementary Information (SI 6) for further details. This trend is important as it shows that the composite properties can be positively influenced and controlled through control of the failure regime.

Furthermore, it should be noted that despite the simplicity of the semi-analytical model, the model captures well the experimental trends, see Figure 5. Improving the quantitative predictions of the model will be a subject of future work. Some possible methods to improve the model will be the implementation of a more refined CZM to better capture the properties of the layer material, and the utilisation of FEA so that the properties of the bricks can be included in the model and more realistic boundary conditions can be applied. In this work we have also shown the importance of defects, or variations in strength, in the layer material on the response of the structure. Another possible method to improve the quantitative predictions of the model is therefore to capture the realistic strength variability of the layer material and implement this into the model

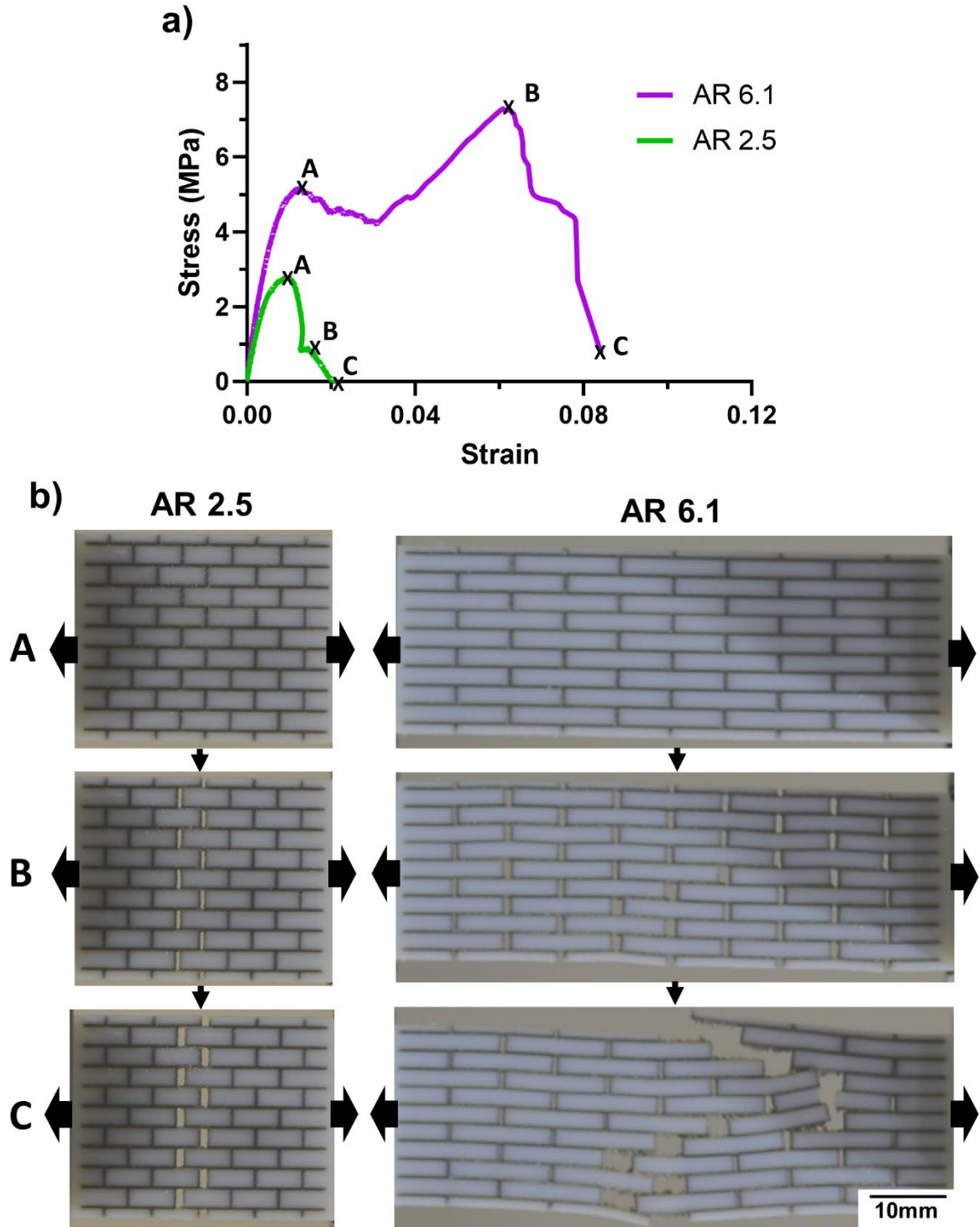


Figure 2: a) Experimental Stress-Strain response of the Brick-and-Mortar structures with Aspect Ratio 2.5 and 6.1, respectively. b) Snapshots of the key failure sequence events in the experiment show two distinct failure regimes; one where failure occurs through the shear layers immediately after the first couple of normal layers have failed (observed for AR 2.5 and labelled ‘two-peak’ failure), and one where failure occurs through the shear layers only after all of the normal layers have failed (observed for AR 6.1 and labelled ‘peak-plateau-peak’ failure).

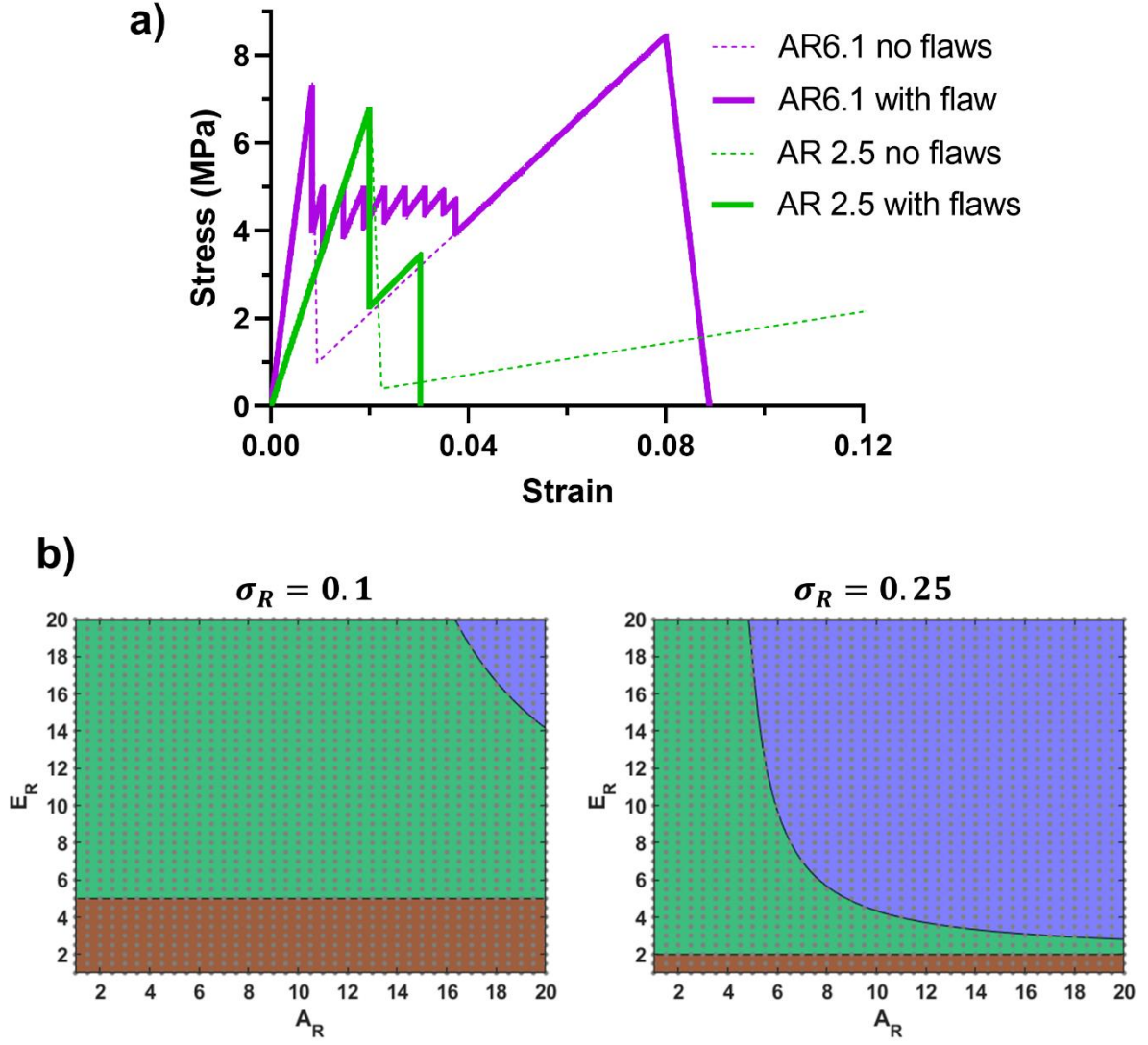


Figure 3: a) Finite-sized semi-analytical model stress-strain response for AR 2.5 (green) and AR 6.1 (purple) with and without a pre-existing flaw (solid line and dotted line, respectively). b) Failure transition maps for varying Aspect Ratio (A_R) and normal-to-shear layer moduli (E_R) for shear-to-normal layer strength ratios (σ_R) of 0.1, and 0.25. In all maps, the dots represent individual model results, and the colours represent the type of failure regime: brown represents ‘shear-only’ failure, green represents ‘two-peak’ failure and purple represents ‘peak-plateau-peak’ failure. (For interpretation of the references to colour in this figure, the reader is referred to the web version of this article).

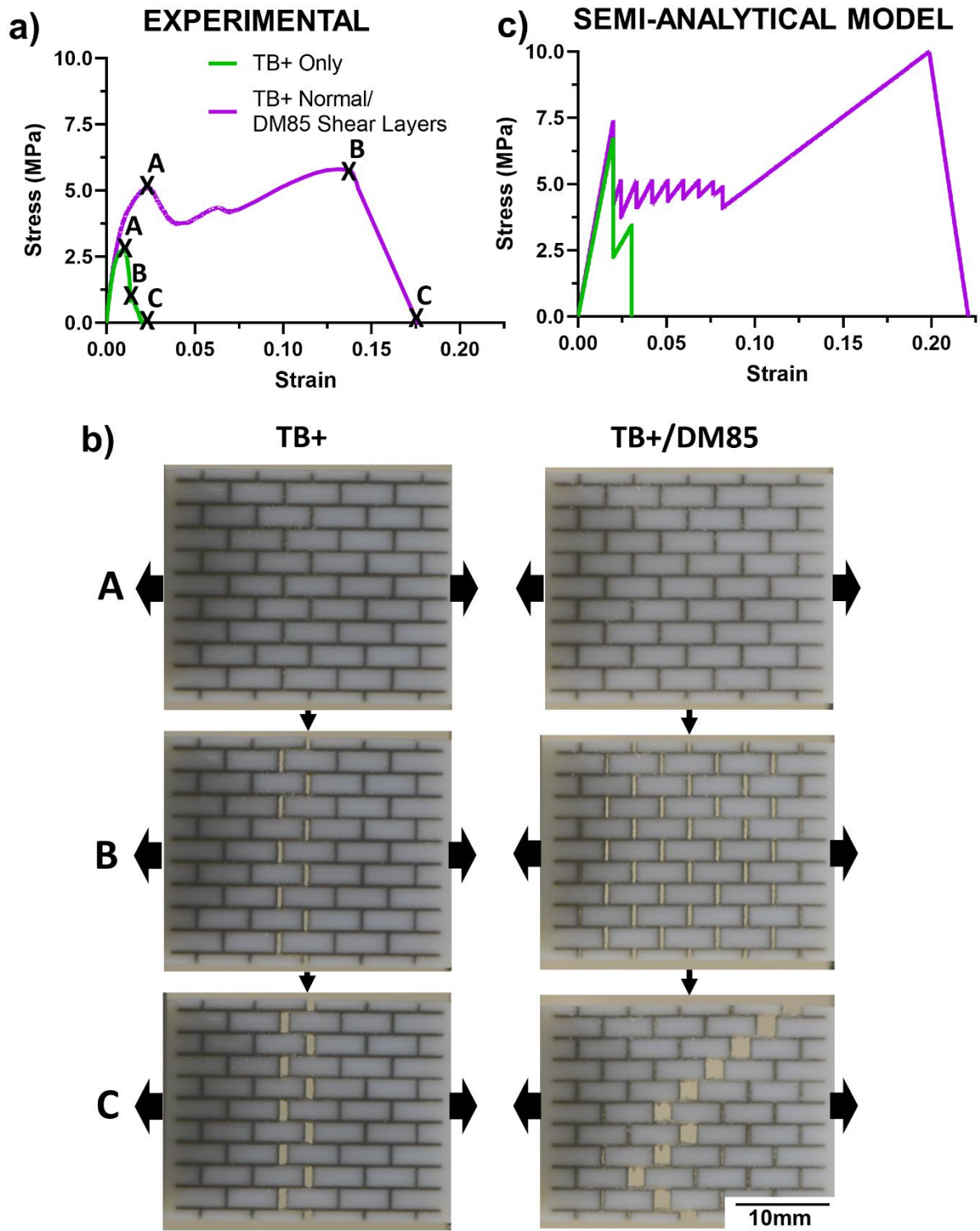


Figure 4: a) Experimental stress-strain response of the Brick-and-Mortar structures with TB+ normal and shear layers, and with TB+ normal layers and DM85 shear layers. b) Snapshots of the key failure sequence events in the experiment show that by strengthening the shear layer from a TB+ layer to a DM85 layer the structure transitions from a 'two-peak' failure regime to a 'peak-plateau-peak' failure regime. c) The semi-analytical model (with a pre-existing flaw) can predict the failure type and the general stress-strain response.

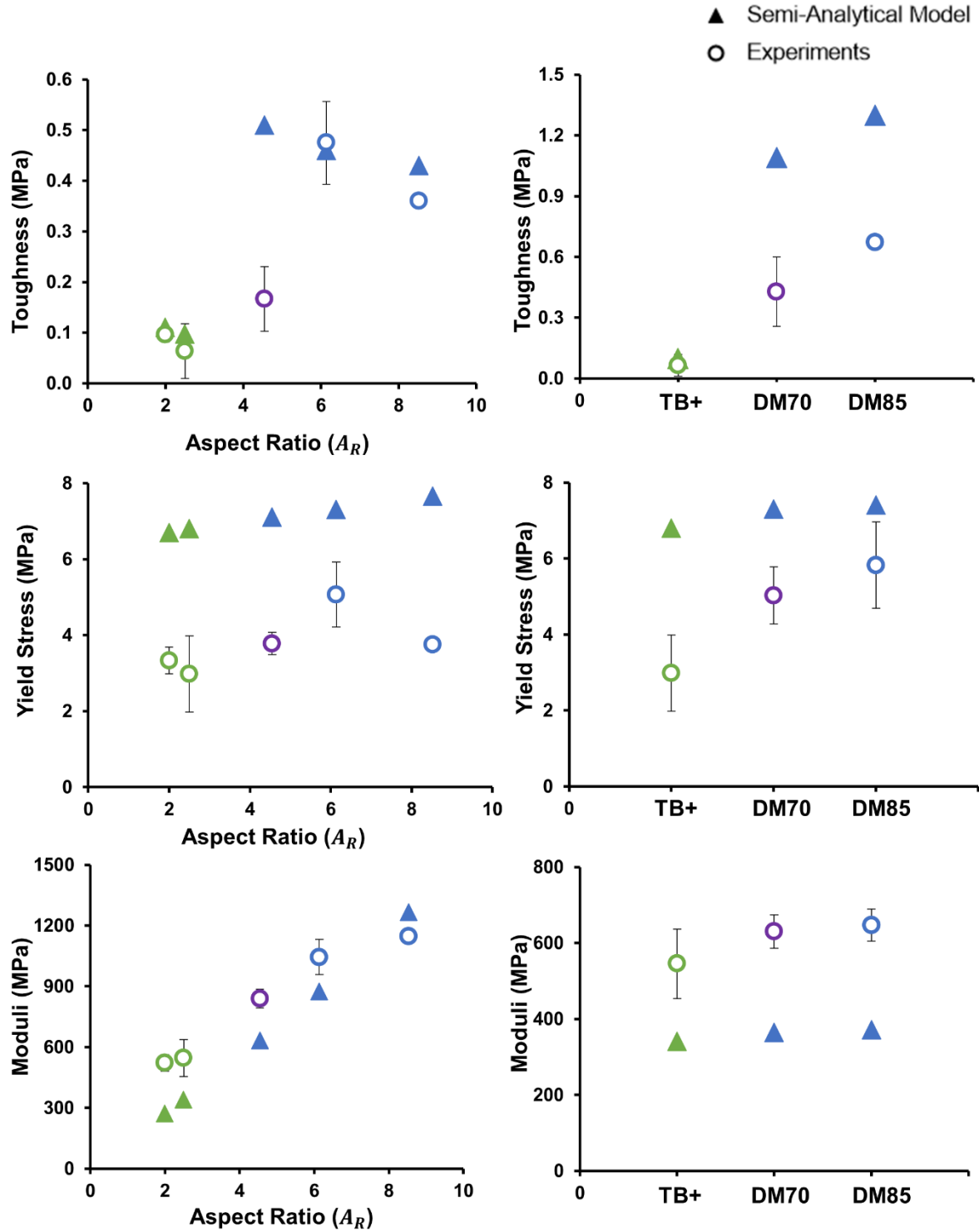


Figure 5: Comparison of semi-analytical model predictions of toughness, yield stress, moduli and type of failure response against experimental results for a range of structures with different aspect ratio and with different normal/shear layer material combinations. Green is used to represent 'two-peak' failure, blue is used to represent 'peak-plateau-peak' failure and purple is used to represent a structure that exhibits a failure response at the transition point between the two failure sequence types. (For interpretation of the references to colour in this figure, the reader is referred to the web version of this article).

5. Conclusion

The present study utilised experimental testing and a newly developed semi-analytical model of finite-sized Brick-and-Mortar structures to reveal the existence of a previously unreported transition between distinct failure regimes: a ‘two-peak’ response and a ‘peak-plateau-peak’ failure response. The ‘two-peak’ failure is characterised by sudden failure of the structure after the first couple of rows of normal layers have failed, while the ‘peak-plateau-peak’ response is characterised by the distribution of damage to all the normal layers prior to full failure of the structure. The two regimes are shown to arise due to the finite-size and inherently flawed nature of the structure. Our work demonstrates that we can control the failure regime to transition from the ‘two-peak’ failure to the ‘peak-plateau-peak’ failure by either increasing the aspect ratio or increasing the strength of the shear layer with respect to the normal layer. Results further identify that a transition to the ‘peak-plateau-peak’ failure regime corresponds to a significant increase in toughness (up to at least 11-fold increase) without compromising the composite strength or stiffness. The identification of these failure regimes in this work, and an understanding of the factors that control these regimes, therefore have important implications on the design of Brick-and-Mortar structures.

Acknowledgements

This research was supported by an Australian Government Research Training Program (RTP) Scholarship, the ATSE Ezio Rizzardo Scholarship and by additional funding from Monash University.

References

1. Chen, P.-Y., J. McKittrick, and M.A. Meyers, *Biological materials: Functional adaptations and bioinspired designs*. Progress in Materials Science, 2012. **57**(8): p. 1492-1704.
2. Ritchie, R.O., *The conflicts between strength and toughness*. Nature Materials, 2011. **10**(11): p. 817-22.
3. Meyers, M.A., et al., *Mechanical strength of abalone nacre: Role of the soft organic layer*. Journal of the Mechanical Behavior of Biomedical Materials, 2008. **1**(1): p. 76-85.
4. Pokroy, B. and E. Zolotoyabko, *Microstructure of natural plywood-like ceramics: a study by high-resolution electron microscopy and energy-variable X-ray diffraction*. Journal of Materials Chemistry, 2003. **13**(4): p. 682-688.
5. Weaver, J.C., et al., *The Stomatopod Dactyl Club: A Formidable Damage-Tolerant Biological Hammer*. Science, 2012. **336**(6086): p. 1275-1280.
6. Currey, J.D., *Bones : Structure and Mechanics*. 2006, Princeton, UNITED STATES: Princeton University Press.
7. Fratzl, P. and R. Weinkamer, *Nature's hierarchical materials*. Progress in Materials Science, 2007. **52**(8): p. 1263-1334.
8. Naleway, S.E., et al., *Structural Design Elements in Biological Materials: Application to Bioinspiration*. Advanced Materials, 2015. **27**(37): p. 5455-5476.
9. Wegst, U.G.K., et al., *Bioinspired structural materials*. Nature Materials, 2015. **14**(1): p. 23-36.
10. Barthelat, F., et al., *On the mechanics of mother-of-pearl: A key feature in the material hierarchical structure*. Journal of the Mechanics and Physics of Solids, 2007. **55**(2): p. 306-337.
11. Djumas, L., et al., *Enhanced Mechanical Performance of Bio-Inspired Hybrid Structures Utilising Topological Interlocking Geometry*. Scientific Reports, 2016. **6**: p. 26706.
12. Dimas, L.S., et al., *Tough Composites Inspired by Mineralized Natural Materials: Computation, 3D printing, and Testing*. Advanced Functional Materials, 2013. **23**(36): p. 4629-4638.
13. Slesarenko, V., et al., *Understanding the strength of bioinspired soft composites*. International Journal of Mechanical Sciences, 2017. **131-132**: p. 171-178.
14. Slesarenko, V., N. Kazarinov, and S. Rudykh, *Distinct failure modes in bio-inspired 3D-printed staggered composites under non-aligned loadings*. Smart Materials and Structures, 2017. **26**(3): p. 035053.
15. Gu, G.X., et al., *Printing nature: Unraveling the role of nacre's mineral bridges*. Journal of the Mechanical Behavior of Biomedical Materials, 2017. **76**: p. 135-144.
16. Gu, G.X., et al., *Biomimetic additive manufactured polymer composites for improved impact resistance*. Extreme Mechanics Letters, 2016. **9**: p. 317-323.
17. Mirzaeifar, R., et al., *Defect-Tolerant Bioinspired Hierarchical Composites: Simulation and Experiment*. ACS Biomaterials Science & Engineering, 2015. **1**(5): p. 295-304.
18. Dimas, L.S. and M.J. Buehler, *Modeling and additive manufacturing of bio-inspired composites with tunable fracture mechanical properties*. Soft Matter, 2014. **10**(25): p. 4436-4442.
19. Frølich, S., et al., *Uncovering Nature's Design Strategies through Parametric Modeling, Multi-Material 3D Printing, and Mechanical Testing* Advanced Engineering Materials, 2017. **19**(6): p. e201600848.
20. Gu, G.X., M. Takaffoli, and M.J. Buehler, *Hierarchically Enhanced Impact Resistance of Bioinspired Composites*. Advanced Materials, 2017. **29**(28): p. 1700060.
21. Zhang, P., M.A. Heyne, and A.C. To, *Biomimetic staggered composites with highly enhanced energy dissipation: Modeling, 3D printing, and testing*. Journal of the Mechanics and Physics of Solids, 2015. **83**: p. 285-300.
22. Abid, N., et al., *Exploring the fracture toughness of tessellated materials with the discrete-element method*. Journal of Applied Mechanics, 2019: p. 1-36.

23. Begley, M.R., et al., *Micromechanical models to guide the development of synthetic 'brick and mortar' composites*. Journal of the Mechanics and Physics of Solids, 2012. **60**(8): p. 1545-1560.
24. Abid, N., J.W. Pro, and F. Barthelat, *Fracture mechanics of nacre-like materials using discrete-element models: Effects of microstructure, interfaces and randomness*. Journal of the Mechanics and Physics of Solids, 2019. **124**: p. 350-365.
25. Abid, N., M. Mirkhalaf, and F. Barthelat, *Discrete-element modeling of nacre-like materials: Effects of random microstructures on strain localization and mechanical performance*. Journal of the Mechanics and Physics of Solids, 2018. **112**: p. 385-402.
26. Barthelat, F. and M. Mirkhalaf, *The quest for stiff, strong and tough hybrid materials: an exhaustive exploration*. Journal of The Royal Society Interface, 2013. **10**(89): p. 20130711.
27. Dimas, L.S. and M.J. Buehler, *Influence of geometry on mechanical properties of bio-inspired silica-based hierarchical materials*. Bioinspiration & Biomimetics, 2012. **7**(3): p. 036024.
28. Wilbrink, D.V., et al., *Scaling of strength and ductility in bioinspired brick and mortar composites*. Applied Physics Letters, 2010. **97**(19): p. 193701.
29. Ghimire, A., et al., *Tunable interface hardening: Designing tough bio-inspired composites through 3D printing, testing, and computational validation*. Composites Part B: Engineering, 2021. **215**: p. 108754.
30. Singh, A., T.S. Sandhu, and S. Pal, *Interplay of various fracture mechanisms in bio-inspired staggered structure*. Mechanics of Materials, 2019. **139**: p. 103215.
31. Dimas, L.S. and M.J. Buehler, *Tough and stiff composites with simple building blocks*. Journal of Materials Research, 2013. **28**(10): p. 1295-1303.
32. Sen, D. and M.J. Buehler, *Structural hierarchies define toughness and defect-tolerance despite simple and mechanically inferior brittle building blocks*. Scientific Reports (Nature Publisher Group), 2011. **1**: p. 35.
33. Liu, F., et al., *Combination of stiffness, strength, and toughness in 3D printed interlocking nacre-like composites*. Extreme Mechanics Letters, 2019: p. 100621.
34. Bass, L., N.A. Meisel, and C.B. Williams, *Exploring variability of orientation and aging effects in material properties of multi-material jetting parts*. Rapid Prototyping Journal, 2016. **22**(5): p. 826-834.
35. Slesarenko, V. and S. Rudykh, *Towards mechanical characterization of soft digital materials for multimaterial 3D-printing*. International Journal of Engineering Science, 2018. **123**: p. 62-72.

Supplementary Information to “Controlling failure regimes in Brick-and-Mortar structures”

Georgia Hunter¹, Lee Djumas¹, Laurence Brassart^{1,2}, Andrey Molotnikov^{1,3}

¹*Department of Materials Science and Engineering, Monash University, Clayton, Australia*

²*Department of Engineering Science, University of Oxford, Oxford, UK*

³*RMIT Centre for Additive Manufacturing, School of Engineering, RMIT University, Melbourne, Australia*
e: Georgia.Hunter@monash.edu

SI 1. Bilinear Cohesive Zone Model Definition

In our model, the deformation and damage response of the soft layers is described using a Cohesive Zone Model (CZM) with bilinear traction separation law. The traction-separation law relates the opening displacement of a layer to the traction acting on either side of the interface. In 2D, the opening displacement is broken down into a single normal (d_n) and single shear (d_s) component, which can be related to the normal (σ) and shear (τ) tractions across the interface surface as follows:

$$\sigma = (1 - D_n) \frac{d_n E_n}{t} \quad (S1)$$

$$\tau = (1 - D_s) \frac{d_s E_s}{t} \quad (S2)$$

where E_n and E_s are effective normal and shear moduli, respectively, and D_n and D_s are damage variables in the normal and shear directions, which are introduced at damage initiation (σ_{max} and τ_{max} for the normal and shear directions, respectively) and monotonically evolves from 0 to 1 as the material is loaded past the point of damage initiation. For the bilinear CZM, the damage variables evolve according to the following rules:

$$D_n = \frac{\frac{G_{IC}}{\sigma_{max}}(d_n - \delta_n^0)}{d_n \left(\frac{G_{IC}}{\sigma_{max}} - \delta_n^0 \right)} \quad (S3)$$

$$D_s = \frac{\frac{G_{IIC}}{\tau_{max}}(d_s - \delta_s^0)}{d_s \left(\frac{G_{IIC}}{\tau_{max}} - \delta_s^0 \right)} \quad (S4)$$

Where δ_n^0 is the value of d_n at the onset of damage (ie. when σ_{max} is reached), δ_s^0 is the value of d_s at the onset of damage (ie. when τ_{max} is reached), G_{IC} is the normal fracture energy and G_{IIC} is the shear fracture energy. A visual representation of the CZM traction-separation law is represented in Figure S1.

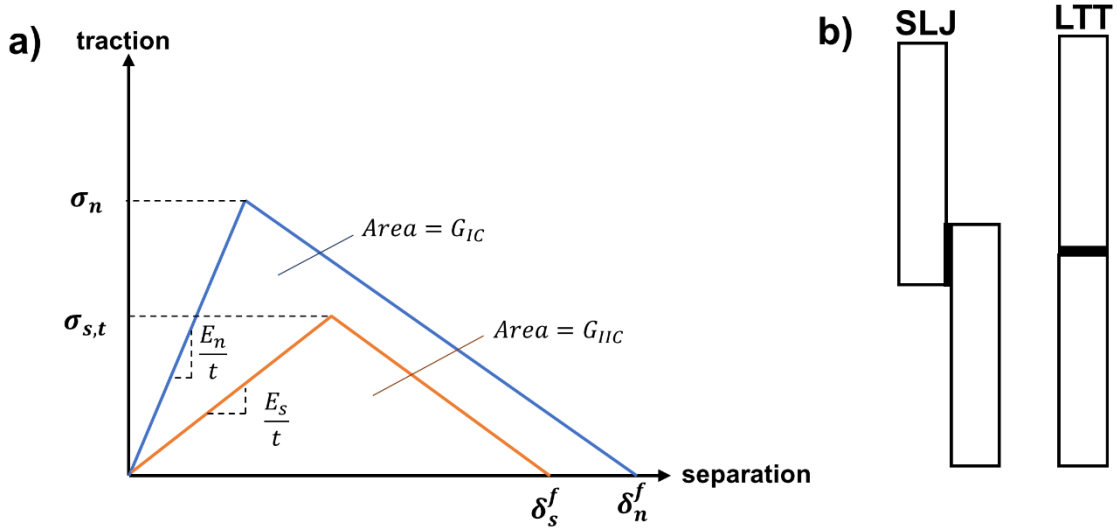


Figure S1: a) A visual representation of the CZM Traction-Separation law used to model the layers, and b) Experimental samples used to calibrate the CZM parameters for TB+, DM70 and DM85. The SLJ sample is used to calibrate the shear parameters and the LTT sample is used to calibrate the normal parameters.

SI 2. Calibration of the Normal and Shear CZM Parameters

Material parameters in the CZM for the TB+, DM70 and DM85 materials were calibrated based on simple experimental tests: Layered Tensile Test (LTT) and Single Lap Joint (SLJ), as shown in Figure S1b. The LTT sample was used to determine the CZM normal parameters, while the SLJ sample was used to calibrate the CZM shear parameters. These two samples were chosen to isolate the shear and normal response of the layer, and thus to avoid any possibility of multiple parameters fitting the same set of results. The samples were also chosen to best capture the homogeneous failure across a layer, which is what is observed experimentally in the Brick-and-Mortar structures. This is opposed to the ‘peeling’ failure mechanism that is captured with a double cantilever beam, which is the sample that is conventionally used to calibrate the normal CZM parameters for adhesive applications.

A representative stress-strain response for the LTT and SLJ tests for TB+, DM70 and DM85, where the strain is the normalisation of displacement by the thickness of the adherend (0.25mm) and the stress is the normalisation of force by the area of the adherend (10x3.125mm), is shown in Figure S2a,b. For comparison, and to illustrate the significant difference in properties between the layer material and the brick material, a representative stress-strain response for the brick material, VW+, as determined using ASTM D638-10, is shown in Figure S2c.

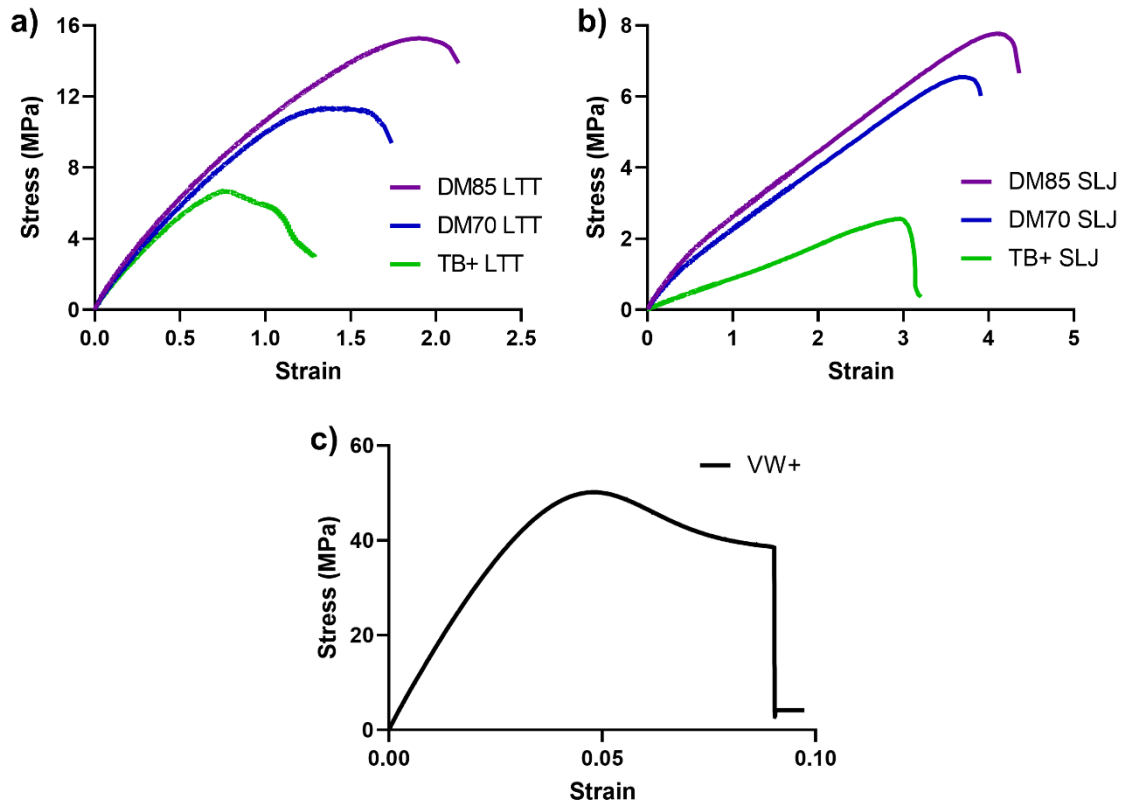


Figure S2: Representative stress-strain response for TB+, DM70 and DM85 for the a) LTT tests and b) SLJ tests and for c) VW+ using a standard tensile test (ASTM D638-10)

Calibration of the CZM parameters to the experimental results was completed by simulating the LTT and SLJ tests using Finite Element Analysis and adjusting the CZM parameters until the numerical results matched up with the experimental results.

SI 3. Defect Size Sensitivity Analysis

The size of the introduced strength defect on the semi-analytical model mechanical response was observed to only affect the yield strength of the structure and had no effect on the failure mechanism. A sensitivity analysis showed that for a defect of 0.1% (in terms of strength reduction of the layer) or smaller there was insignificant differences in the predicted yield stress, see Figure S3. Therefore, a defect of 0.1% was used for the semi-analytical model in this study.

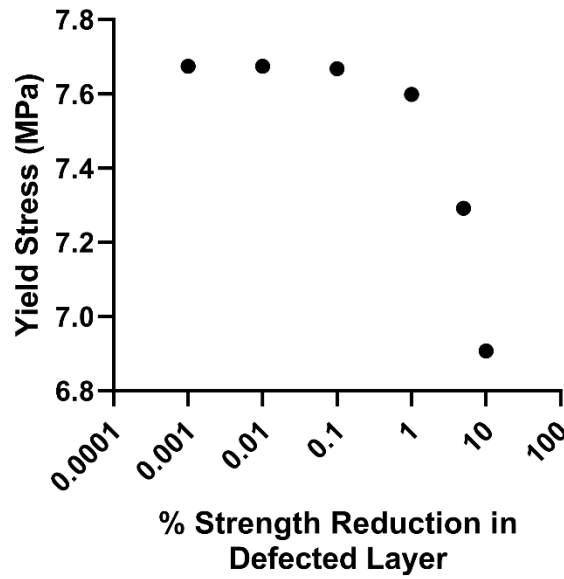


Figure S3: Brick-and-Mortar finite-size analytical model yield stress for different size defects. The size of the defect is defined by the % strength reduction in the defected layer.

SI 4. Size Effect of Semi-Analytical Model

To determine if the number of bricks affects the results of the semi-analytical model, the model was run with 11, 21 and 31 bricks (5, 10 and 15 cells, respectively) for the AR 2.5 and AR 6.1 structure with TB+ layers. The stress-strain response for the AR 2.5 structure, see Figure S4a, shows the same failure mechanism of ‘two-peak’ failure for all sizes, however there is a noticeable decrease in strain for the second peak in the stress-strain response. This is because after the first couple of normal layers have failed, stress concentrates around the layers near the failed normal layers, (ie. the shear layers between the failed normal layers and the next normal layers across from the already failed normal layers). As the size of the structure is increased, the corresponding displacement is normalised to strain over a larger structure length, thus resulting in a smaller strain to the next failure event (which for this failure mechanism is failure of the shear layers, resulting in full failure of the structure).

The stress-strain response for the AR 6.1 structure also shows the same failure mechanism for all sizes: a ‘peak-plateau-peak’ failure, see Figure S4b. As the number of bricks increases, the number of mini peaks in the ‘plateau’ region increase. This is because each mini peak corresponds to a row of normal layers failing, and an increase in the size means there are more normal layers to fail and hence there are more mini peaks. However, significantly, the top of

the mini peaks is the same for all size structures, and the two major peaks are the same for all sizes.

Despite the slight differences in some components of the stress-strain plot, the predicted failure mechanism is consistently the same for all sizes for a particular set of parameters. Therefore, any size can be chosen for use in the analytical model to capture the failure mechanism. For this study, 21 bricks (10 cells) was chosen to capture the representative failure mechanism behaviour for a particular set of parameters.

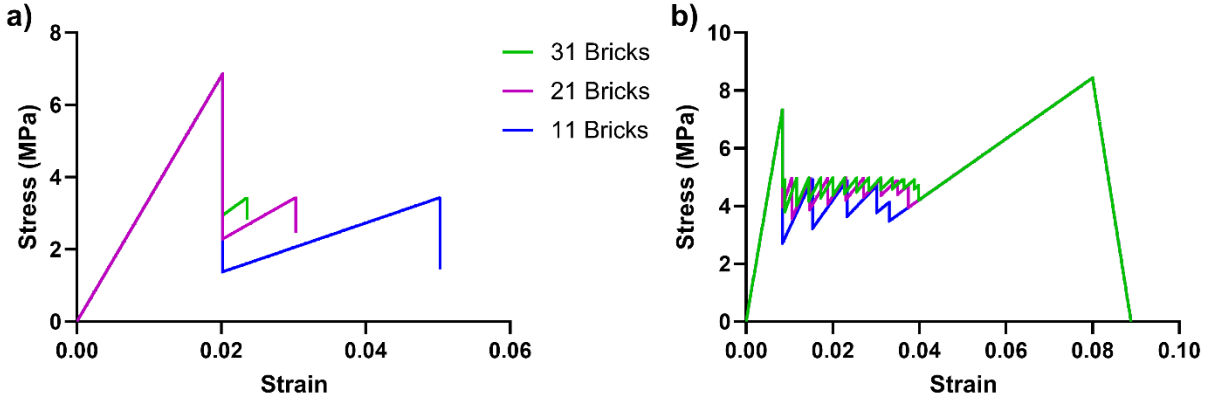


Figure S4: Brick-and-Mortar finite-size analytical model stress-strain response for 11, 21 and 31 bricks for a) AR 2.5 structure and b) AR 6.1 structure, with TB+ CZM parameters.

SI 5. Derivation of Failure Sequence Transition Criteria

The difference between ‘shear-only’ failure and ‘two-peak’ failure is whether the normal or shear layers fail first. The transition point is therefore when the ratio of the shear-to-normal layer stress is equal to the ratio of the shear-to-normal layer strength: *ie.* $\tau_{max}/\sigma_n = \tau/\sigma$. From the geometry of the structure, in the elastic region $d_n = 2d_s$, which equates to $\tau/\sigma = E_s/2E_n$. Therefore, the transition point between ‘shear-only’ failure and ‘two-peak’ failure is when $\tau_{max}/\sigma_n = E_s/2E_n$.

The difference between ‘two-peak’ failure and ‘peak-plateau-peak’ failure is whether, after the first couple of normal layers have failed, the next failure event is failure of the shear layer between the already failed normal layers or failure of the normal layers adjacent to the already failed normal layers, respectively. To determine an analytical relation for the transition point let us therefore consider a structure where three adjacent normal layers in the middle of the Brick-and-Mortar structure have failed already. The transition point is therefore when the stress

in the shear layer that is between the already failed normal layers is equal to the stress in the normal layer that is directly adjacent to the already failed normal layers. For a structure with 3 unit cells (7 bricks), this occurs when $\frac{\tau_{max}}{\sigma_n} = \frac{1}{2E_R} + \frac{1}{A_R} + \frac{1}{2(E_R+A_R)}$. Repeating this analysis for larger structures slightly changes the exact transition point, however it does not change how the transition point trends with changing the structure parameters. As it is predominantly these trends that we are interested in, then the analytical relation determined from the consideration of 3 unit cells is used for the transition point. It should also be noted that the analytical model is very quick to run (runs in seconds), and therefore this relation can be used to approximate the transition point for a particular set of parameters and the exact transition point predicted for a structure with a particular number of unit cells can then be determined by tuning the parameters around the approximated transition point.

SI 6. Derivation of Analytical Equations Relating Composite Properties and Structure Parameters

Composite Initial Moduli

The initial composite moduli can be determined from the single unit cell construction, assuming the flaws of the structure only lie within the strength of the layers and not the moduli of the layers. In a single unit cell, in the undamaged region, the composite stress is equal to $\sigma_{comp} = \frac{E_s d_T}{t} \left(E_R + \frac{A_R}{4} \right)$ and the strain is equal to $\varepsilon_T = d_T / (w + t)$. Therefore, the initial composite moduli for the structure is $E_{Comp} = \frac{E_s(w+t)}{t} \left(\frac{A_R}{4} + E_R \right)$. This is valid for all failure sequence types.

Composite Yield Strength

The composite yield strength is defined as the composite stress when the first damage occurs in the structure. For the ‘shear-only’ failure mechanism this is when the first shear layer reaches τ_{max} , while for the ‘two-peak’ and ‘peak-plateau-peak’ failure response this is when the first normal layer reaches σ_{max} .

For the ‘shear-only’ failure mechanism, the first shear layer reaches τ_{max} at $d_s = \tau_{max} t / E_s$. At this displacement, the normal strength in the normal layers is $\sigma = E_n d_s / 2t$. Subsequently, the composite yield stress is $\sigma_Y = \tau_{max} \left(\frac{A_R}{2} + 2E_R \right)$ and the yield stress occurs at a strain of $\varepsilon_Y = \frac{2\tau_{max} t}{E_s(w+t)}$.

For the ‘two-peak’ and ‘peak-plateau-peak’ failure response, the first normal layer reaches σ_{max} at $d_n = \sigma_{max} t / E_n$. At this displacement, the shear strength in the shear layers is $\tau = 2E_s d_n / t$. Subsequently, the composite yield stress is $\sigma_Y = \sigma_{max} \left(\frac{A_r}{4} + E_R \right)$ and the yield stress occurs at a strain of $\varepsilon_Y = \frac{\sigma_{max} t}{E_n(w+t)}$.

Composite Toughness

To determine a simplified expression that relates the structure parameters to the toughness (here defined as the area under the stress-strain curve) of the structure, we can simplify the stress-strain response for each failure type. For the ‘shear-only’ failure the response is simplified to a single peak, for the ‘two-peak’ failure the response is simplified to capture only the first peak (which assumes the structure is large enough that the second peak is insignificant, as seen in the size effect study), and for the ‘peak-plateau-peak’ failure the response is simplified to a peak, a straight plateau and a second peak. These simplifications are visually shown in Figure S5.

For the ‘shear-only’ and ‘two-peak’ failure responses the toughness is therefore simply $\sigma_Y \varepsilon_Y / 2$, which correlates to $T = \frac{\tau_{max}^2 t}{E_s(w+t)} \left(\frac{A_r}{2} + 2E_R \right)$ for ‘shear-only’ failure and $T = \frac{1}{2} \left(\frac{t \sigma_{max}^2}{(t+w)E_n} \right) \left(\frac{A_r}{4E_R} + 1 \right)$ for ‘two-peak’ failure.

For the ‘peak-plateau-peak’ failure response, the toughness is determined from the relation: $T = \frac{\sigma_Y \varepsilon_Y}{2} + \frac{\sigma_P (\varepsilon_P - \varepsilon_Y)}{2} + \frac{(\varepsilon_T - \varepsilon_P)(\sigma_T + \sigma_P)}{2}$. The plateau stress, σ_P , can be approximated as the composite stress when the second set of normal layers start to fail (where the first set of normal layers that fail are the ones that correspond to the first major peak). To calculate this, we consider a structure where three adjacent normal layers in the middle of the Brick-and-Mortar structure have failed already and determine the composite stress when the adjacent normal layers reach σ_{max} : ie. $\sigma_P = \frac{A_r \sigma_n}{4E_c} \left(\frac{1}{2E_R} + \frac{1}{A_r} + \frac{1}{2(E_R + A_r)} \right)$. The linear increase up to the second peak corresponds to when all the normal layers have failed and only the shear layers remain intact. The composite stress during this region therefore simplifies to $\sigma_c = \tau w / 2h$. The peak occurs when the shear layers reach τ_{max} , which correlates to a peak composite stress of $\sigma_T = \tau_{max} A_r / 2$ at a strain of $\varepsilon_T = \frac{2t \sigma_s}{E_s(w+t)}$. Finally, the strain that correlates to the end of the plateau region can be approximated by determining the strain in the structure when the plateau stress equals the composite stress of a structure with only shear layers intact, ie. $\varepsilon_P =$

$\frac{4\sigma_P}{t(w+t)E_sA_R}$. Combining all these expressions, the toughness in the ‘peak-plateau-peak’ failure response is approximated by $T = \left(\frac{t\sigma_{max}^2}{(t+w)E_n} \right) \left(\frac{1}{2} + \frac{A_R E_R \sigma_R^2}{2} \right)$.

Similar to the analytical relations that were derived to predict the failure sequence transition, these analytical relations for toughness are only an approximated solution to capture the trends between structure parameters and toughness. A more accurate toughness prediction can be quickly and easily obtained by running the full analytical model.

Visual Representation of Composite Property Trends

A visual representation of the relationship between composite parameters (A_R , E_R and σ_R) and the composite properties (normalised toughness, strength and moduli) are shown in Figure S6. These plots were constructed by running the analytical model for a range of A_R parameters (between 1 and 20, in increments of 1), for four different E_R values (2, 8, 14, 20) and for two different σ_R values (0.25 and 0.5). The results for a single σ_R value are presented in each plot and for each σ_R value two plots were constructed to demonstrate the key trends: normalised moduli vs normalised toughness and normalised strength vs normalised toughness. Within each plot, each dot represents a single analytical model result, with colours identifying the failure mechanism type for that result: red for ‘shear-only’ failure, green for ‘two-peak’ failure and blue for ‘peak-plateau-peak’ failure. All results that lie on a solid line correspond to constant E_R value (as labelled) and changing A_R . While dashed lines are used to show the results for a constant A_R value and changing E_R (Note, for simplicity, only three dashed lines are shown that correspond to $A_R = 1, 10, 20$, however the dashed lines for the rest of the A_R results can be logically determined from these). The resulting plots show there is a clear jump in toughness for all combinations of parameters when transitioning from a ‘two-peak’ failure to a ‘peak-plateau-peak’ failure, without compromising the trends of the stiffness and strength of the structure.

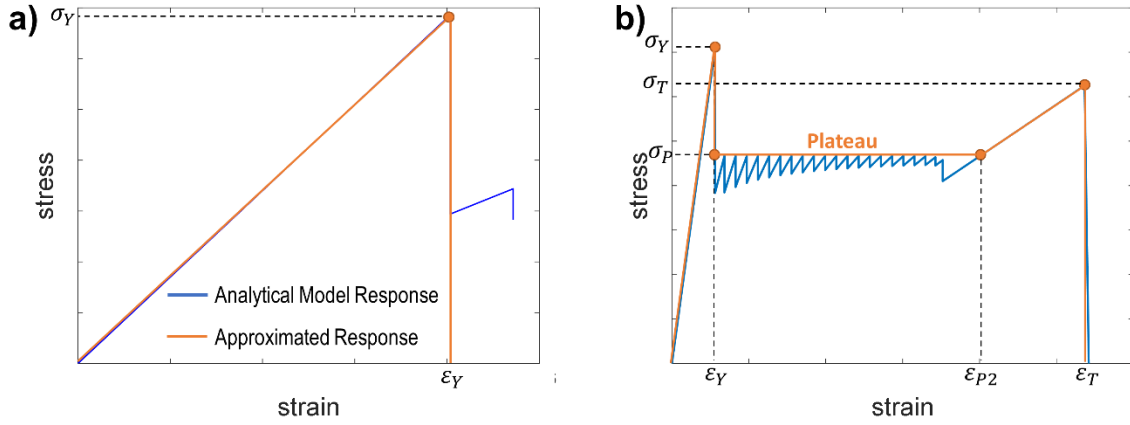


Figure S5: Approximation of the stress-strain response for a) ‘Shear-only’ failure and ‘Two-peak’ failure and b) ‘Peak-plateau-peak’ failure, plotted against the actual analytical model stress-strain response.

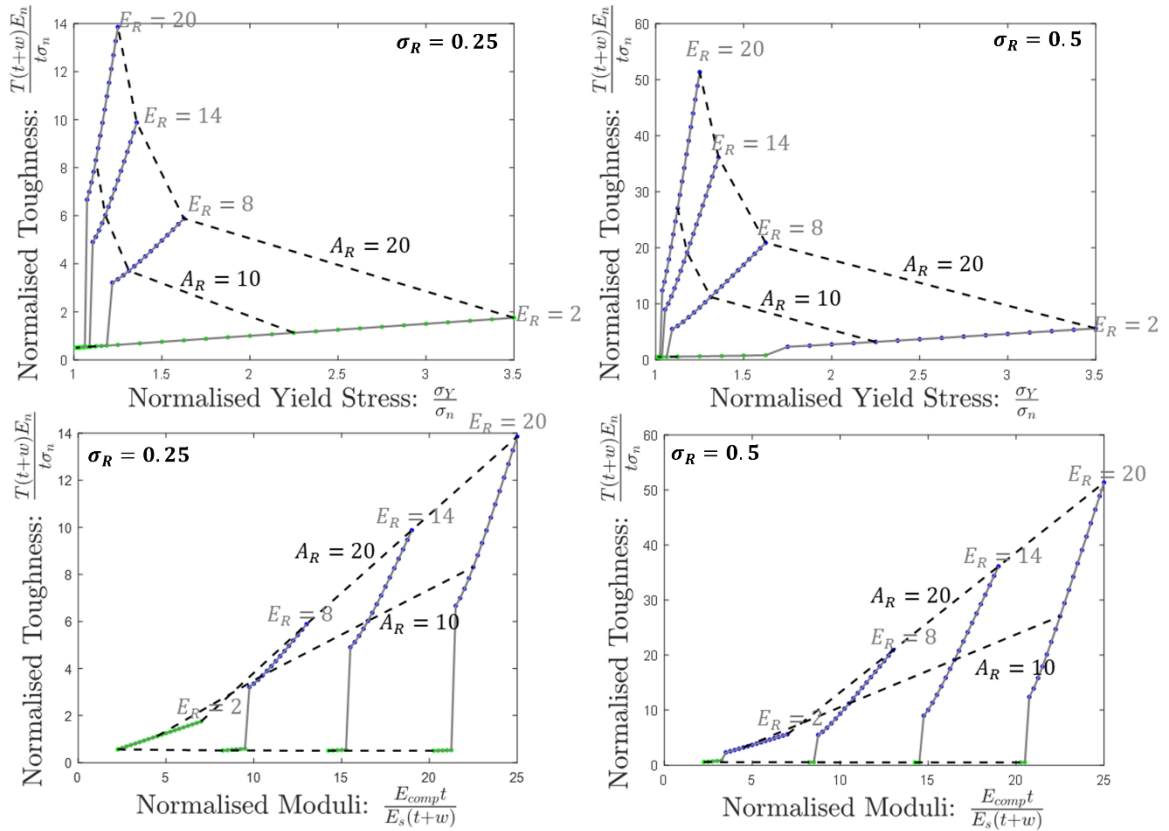


Figure S6: Composite property maps (normalised toughness vs normalised strength and normalised toughness vs normalised moduli) for varying A_R (dashed line: $A_R = 1 - 20$) and E_R (solid line: $E_R = 2, 8, 14, 20$) and for σ_R of 0.25 and 0.5. In all maps, the dots represent an analytical model result, and the colours represent the type of failure regime: red represents ‘shear-only’ failure, green represents ‘two-peak’ failure and blue represents ‘peak-plateau-peak’ failure. (For interpretation of the references to colour in this figure, the reader is referred to the web version of this article).